2024 European Control Conference (ECC)
June 25-28, 2024. Stockholm, Sweden

Data-Adaptive Retrofit Control for Power System Stabilizer: Refinement with Park Model of Synchronous Generators

Saw Kay Khine Oo and Takayuki Ishizaki

***Abstract*—In this paper, we extend the design of data-adaptive retrofit control for power system stabilizers (PSS) from the one-axis generator model to the Park generator model, which is the most detailed representation of synchronous generators. The data-adaptive retrofit control allows individual sub-controller designers to design and implement PSS, using only a local subsystem model and local measurements. The data-adaptive PSS can also adapt to the variation of grid characteristics through the process of real-time estimation of intricate dynamical feedback effects between the main grid and the generator states. This paper presents the details of an extended retrofit control method that accounts for the higher order dynamics and increased parameters of the Park generator model. In addition, we perform a multi-objective optimization for online identification of grid characteristics to improve the performance of the PSS. Finally, we demonstrate the efficacy of the proposed data-adaptive PSS by conducting a detailed numerical simulation on the IEEE 68-bus power system model composed of the Park generator models, resulting in a large-scale complex nonlinear differential algebraic equation system.**

I. Introduction

Power system stabilizers (PSS) are decentralized controllers in power systems that generate control signals for automatic voltage regulators (AVR) of generator excitation systems. They are important to damp frequency oscillations caused by disturbances and improve the transient stability of the power system. Industry-standard conventional PSS, designed with a lead-lag structure have significantly contributed to enhancing power system stability [1], [2]. Numerous research efforts have been dedicated to optimizing parameters for conventional PSS, utilizing techniques such as genetic algorithms, tabu search, and particle swarm optimization [3]–[5]. These methods effectively fine-tune the parameters in conventional PSS but lack the flexibility to adapt to diverse conditions. Recently, [6], [7] proposed PSS design methods that aim to enhance performance by adapting to dynamic grid characteristics. While these modern PSSs were designed to be adaptive, they were only validated using the single machine connected to infinite bus. For the adaptive PSS with the application in multi-machine power system, neural network based adaptive PSS [8], [9] were introduced. However, there is still a concern regarding active modifications made to the design of PSS as these changes may potentially result in the destabilization of the entire power system, particularly when implemented in large-scale power systems.

Data-adaptive retrofit control for PSS, employing the one-axis generator model has been introduced in the study [10] to address the issues of PSS design procedure, which include a lack of consideration for variations in grid characteristics and the potential destabilization of the entire power system through active modifications. The study addressed those issues by online identification of a dynamic feedback effect between the states of a generator and the main grid, and by the use of retrofit control approach [11]–[14] that ensures the stability of the power system. The details of the retrofit control approach for data-adaptive PSS design will be explained in Section III. Even though the study validated the efficacy of data-adaptive retrofit control for PSS designed with the one-axis generator model using the IEEE 9-bus power system model, we identify two main concerns regarding practicality.

1) The existing data-adaptive retrofit control for PSS is designed based on the one-axis generator model, which is a reduced-order model, and therefore may not have optimal performance in real-world applications.
2) The IEEE 9-bus power system model is a small-scale model that may significantly differ from that in real-life large-scale power systems.

In this paper, we address concern 1) by extending the data-adaptive retrofit control using the Park generator model, which is the most detailed representation of synchronous generators. We aim to resolve concern 2) by conducting a detailed numerical simulation on the IEEE 68-bus model to assess the practical significance of data-adaptive retrofit control on one of the large-scale power system models during the fault occurrence. These considerations are the main practical contributions of this paper.

This paper is organized as follows. In Section II, we describe the power system model discussed in this paper. In Section III, we review the existing data-adaptive retrofit control approach using the one-axis generator model. In Section IV, we present the details of an extended data-adaptive retrofit control using the Park generator model. In Section V, we examine the efficacy of the proposed PSS through a numerical demonstration on the IEEE 68-bus system. In Section VI, we provide the concluding remarks.

II. Power System Model

In this section, we review a standard power system model. The same model will be used for the numerical simulation in Section V. The details can be found in [15] while the standard values of the generators are taken from [16].

A. Park Model of a Synchronous Generator

The detailed representation of a synchronous generator is modeled using Park's transformation, while reduced-order modelings, such as one-axis and classical models are often

used for research purposes. In this paper, a synchronous generator is described with thePark model.

Let $E_{\mathrm{q}i}$ denote the internal voltage due to field winding and $E_{\mathrm{d}i}, \psi_{\mathrm{d}i}$ and $\psi_{\mathrm{q}i}$ denote internal voltages due to three damper windings of the generator connected to Bus i. Let δ_i denote the generator's rotor angle relative to the frame rotating at the standard angular frequency ω_0. The bus voltage phasor $\boldsymbol{V}_i$ and the bus current phasor $\boldsymbol{I}_i$ of the network reference frame are given as

$$\boldsymbol{V}_i = (V_{\mathrm{d}i} + \boldsymbol{j} V_{\mathrm{q}i}) e^{j(\delta_i - \frac{\pi}{2})}, \quad \boldsymbol{I}_i \ = (I_{\mathrm{d}i} + \boldsymbol{j} I_{\mathrm{q}i}) e^{j(\delta_i - \frac{\pi}{2})} \tag{1a}$$

where $V_{\mathrm{d}i}$ and $V_{\mathrm{q}i}$ are real and imaginary parts of Bus i voltage; $I_{\mathrm{d}i}$ and $I_{\mathrm{q}i}$ are real and imaginary parts of Bus i current on the machine reference frame, described as

$$\begin{aligned} V_{\mathrm{d}i} &= |\boldsymbol{V}_i| \sin(\delta_i - \angle \boldsymbol{V}_i), \quad V_{\mathrm{q}i} = |\boldsymbol{V}_i| \cos(\delta_i - \angle \boldsymbol{V}_i) \\ I_{\mathrm{q}i} &= \tfrac{-(X''_{\mathrm{q}i} - X_{\mathrm{ls}i})}{X''_{\mathrm{q}i}(X'_{\mathrm{q}i} - X_{\mathrm{ls}i})} E_{\mathrm{d}i} + \tfrac{(X'_{\mathrm{q}i} - X''_{\mathrm{q}i})}{X''_{\mathrm{q}i}(X'_{\mathrm{q}i} - X_{\mathrm{ls}i})} \psi_{\mathrm{q}i} + \tfrac{V_{\mathrm{d}i}}{X''_{\mathrm{q}i}} \\ I_{\mathrm{d}i} &= \tfrac{(X''_{\mathrm{d}i} - X_{\mathrm{ls}i})}{X''_{\mathrm{d}i}(X'_{\mathrm{d}i} - X_{\mathrm{ls}i})} E_{\mathrm{q}i} + \tfrac{(X'_{\mathrm{d}i} - X''_{\mathrm{d}i})}{X''_{\mathrm{d}i}(X'_{\mathrm{d}i} - X_{\mathrm{ls}i})} \psi_{\mathrm{d}i} - \tfrac{V_{\mathrm{q}i}}{X''_{\mathrm{d}i}} \end{aligned} \tag{1b}$$

where $X''_{\mathrm{d}i}, X'_{\mathrm{d}i}$ denote sub-transient and transient reactance of d-axis, $X''_{\mathrm{q}i}, X'_{\mathrm{q}i}$ denote sub-transient and transient reactance of q-axis, and $X_{\mathrm{ls}i}$ denotes the leakage reactance of the generator connected to Bus i.

The relation between $\boldsymbol{V}_i$ and $\boldsymbol{I}_i$ can be derived from (1a) and (1b). Active power P_i and reactive power Q_i of Bus i can be defined as the real and imaginary parts of $\boldsymbol{V}_i \overline{\boldsymbol{I}}_i$, namely

$$\begin{aligned} P_i &= V_{\mathrm{q}i} I_{\mathrm{q}i} + V_{\mathrm{d}i} I_{\mathrm{d}i} \\ Q_i &= V_{\mathrm{q}i} I_{\mathrm{d}i} - V_{\mathrm{d}i} I_{\mathrm{q}i}. \end{aligned} \tag{1c}$$

The dynamics of the Park generator model, with the subscript "i" neglected for simplicity, are described as

$$\begin{cases} \dot{\delta} = \omega_0 \omega \\ M\dot{\omega} = -D\omega - P + P^*_{\mathrm{m}} \\ T'_{\mathrm{do}} \dot{E}_{\mathrm{q}} = -E_{\mathrm{q}} - (X_{\mathrm{d}} - X'_{\mathrm{d}}) \Big[I_{\mathrm{d}} - \frac{X'_{\mathrm{d}} - X''_{\mathrm{d}}}{(X'_{\mathrm{d}} - X_{\mathrm{ls}})^2} \\ \qquad\qquad (\psi_{\mathrm{d}} + (X'_{\mathrm{d}} - X_{\mathrm{ls}}) I_{\mathrm{d}} - E_{\mathrm{q}}) \Big] + V_{\mathrm{fd}} \\ T''_{\mathrm{do}} \dot{\psi}_{\mathrm{d}} = -\psi_{\mathrm{d}} + E_{\mathrm{q}} - (X'_{\mathrm{d}} - X_{\mathrm{ls}}) I_{\mathrm{d}} \\ T'_{\mathrm{qo}} \dot{E}_{\mathrm{d}} = -E_{\mathrm{d}} + (X_{\mathrm{q}} - X'_{\mathrm{q}}) \Big[I_{\mathrm{q}} - \frac{X'_{\mathrm{q}} - X''_{\mathrm{q}}}{(X'_{\mathrm{q}} - X_{\mathrm{ls}})^2} \\ \qquad\qquad (\psi_{\mathrm{q}} + (X'_{\mathrm{q}} - X_{\mathrm{ls}}) I_{\mathrm{q}} + E_{\mathrm{d}} \Big] \\ T''_{\mathrm{qo}} \dot{\psi}_{\mathrm{q}} = -\psi_{\mathrm{q}} - E_{\mathrm{d}} - (X'_{\mathrm{q}} - X_{\mathrm{ls}}) I_{\mathrm{q}} \end{cases} \tag{1d}$$

where ω is the angular frequency deviation relative to the standard angular frequency ω_0, while M, D and P^*_{m} are inertia constant, damping coefficient and mechanical input respectively. $X_{\mathrm{d}}, X_{\mathrm{q}}$ are synchronous reactances of d-axis and q-axis respectively, $T''_{\mathrm{do}}, T'_{\mathrm{do}}$ are sub-transient and transient open-circuit time constants of d-axis respectively, $T''_{\mathrm{qo}}, T'_{\mathrm{qo}}$ are sub-transient and transient open-circuit time constants of q-axis respectively, and V_{fd} is the field voltage input. The mechanical input P^*_{m} is supposed to be constant to maintain ω_0 at equilibrium, while the field voltage input V_{fd} from the automatic voltage regulator (AVR) is considered as a control input that will be described in Section II-C.

For comparison, we introduce the following dynamics of the one-axis generator model, given as

$$\begin{cases} \dot{\delta} = \omega_0 \omega \\ M\dot{\omega} = -D\omega - P + P^*_{\mathrm{m}} \\ T'_{\mathrm{do}} \dot{E}_{\mathrm{q}} = -\frac{X_{\mathrm{d}}}{X'_{\mathrm{d}}} E_{\mathrm{q}} + (\frac{X_{\mathrm{d}}}{X'_{\mathrm{d}}} - 1) |\boldsymbol{V}| \cos(\delta - \angle \boldsymbol{V}) + V_{\mathrm{fd}} \end{cases} \tag{2}$$

where the dynamics of the four states E_{q}, E_{d}, ψ_{q}, and ψ_{d} in (1d) are reduced to the dynamics of the single state E_{q}. For this simplified model, (1b) can also be simplified as

$$I_{\mathrm{q}} = \tfrac{-E_{\mathrm{d}} + V_{\mathrm{d}}}{X'_{\mathrm{q}}}, \quad I_{\mathrm{d}} \ = \tfrac{E_{\mathrm{q}} - V_{\mathrm{q}}}{X'_{\mathrm{d}}}. \tag{3}$$

The one-axis generator model is used in Section III only for review purposes while the Park generator model is used to demonstrate the main practical contributions in Sections IV and V.

B. Power System Stabilizer Model

The main purpose of the PSS is to generate an input to the automatic voltage regulator (AVR), denoted as V_{pss}. We introduce the following standard PSS model used in [17].

$$\begin{aligned} \dot{x}_{\mathrm{pss}} &= A_{\mathrm{pss}} x_{\mathrm{pss}} + B_{\mathrm{pss}} \omega \\ V_{\mathrm{pss}} &= C_{\mathrm{pss}} x_{\mathrm{pss}} + D_{\mathrm{pss}} \omega \end{aligned} \tag{4}$$

where x_{pss} is denoted as $x_{\mathrm{pss}} := [x_{\mathrm{pss1}}\ x_{\mathrm{pss2}}\ x_{\mathrm{pss3}}]^\intercal$ that consists of three state variables of PSS and $A_{\mathrm{pss}}, B_{\mathrm{pss}}, C_{\mathrm{pss}}, D_{\mathrm{pss}}$ are the state matrices composed of PSS gain and time constants.

C. Automatic Voltage Regulator Model

An AVR is attached to every generator in the power system to produce the external input V_{fd} in (1d). We refer to a combination of the data-adaptive PSS and the standard PSS as a refined PSS. The model of AVR with refined PSS is described as

$$\begin{cases} \tau \dot{V}_{\mathrm{fd}} = -V_{\mathrm{fd}} + k_{\mathrm{ap}} (V^*_{\mathrm{ref}} - |\boldsymbol{V}| + V_{\mathrm{pss}} - V_{\mathrm{pss,re}} - u_{\mathrm{ext}}) \\ V^*_{\mathrm{ref}} = \frac{V^*_{\mathrm{fd}}}{k_{\mathrm{ap}}} + |\boldsymbol{V}|^* \end{cases} \tag{5}$$

where $V_{\mathrm{pss,re}}$ is the control input produced by the data-adaptive PSS based on retrofit control.

D. Load Model

Let z^*_{load} denote as a load impedance and we use the constant impedance model given as

$$\boldsymbol{I} = -\tfrac{\boldsymbol{V}}{z^*_{\mathrm{load}}}. \tag{6}$$

E. Transmission Network Model

A transmission network of N buses is represented by

$$\begin{bmatrix} \boldsymbol{I}_1 \\ \vdots \\ \boldsymbol{I}_N \end{bmatrix} = \underbrace{\begin{bmatrix} \boldsymbol{Y}_{11} & \cdots & \boldsymbol{Y}_{1N} \\ \vdots & \ddots & \vdots \\ \boldsymbol{Y}_{N1} & \cdots & \boldsymbol{Y}_{NN} \end{bmatrix}}_{\boldsymbol{Y}} \begin{bmatrix} \boldsymbol{V}_1 \\ \vdots \\ \boldsymbol{V}_N \end{bmatrix}, \tag{7}$$

where $\boldsymbol{Y}_{ij}$ is the admittance between Bus i and Bus j, and $\boldsymbol{Y}$ is the admittance matrix. The power system model in

this paper is represented as a differential-algebraic equation (DAE) model where the generators in (1) and the loads in (6) are interconnected by the algebraic equation in (7).

III. Review of Data-Adaptive Retrofit Control

A. System Description and Controller Design

In this sub-section, we review the design of data-adaptive PSS using the one-axis generator model proposed in [10]. In the retrofit control framework, the system is divided into a "local linear subsystem G", which is the linear part of a single generator assumed to be controlled by a local decision maker or a generator owner, and an "environment $\overline{G}$", which represents the main grid connected to the generator and assumed to be unknown to the generator owner. The entire power system is regarded as the feedback connection of a local linear subsystem G and an environment $\overline{G}$ given as

$$G : \begin{cases} \dot{x} = Ax + Bu + Lv \\ w = \Gamma x \end{cases} \tag{8}$$

$$\overline{G} : \begin{cases} \dot{\bar{x}} = f_{\mathrm{p}}(\bar{x}, w) \\ v = g_{\mathrm{p}}(\bar{x}, w) \end{cases} \tag{9}$$

where x and $\bar{x}$ are the internal states of the local linear subsystem and the environment respectively, v and w are interaction signals, A, B, L and Γ are system matrices of G, and f_{p} and g_{p} are smooth functions.

The generator owner has access to the system constants and internal states of their own generator, AVR and standard PSS. In addition, the generator owner can also measure the exogenous inputs P_{m} and $\boldsymbol{V}$ affecting their generator and AVR. Therefore, interaction signals can be obtained. An operating point of interest or equilibrium is defined as $(x^*, \bar{x}^*)$ that satisfies the following conditions

$$0 = Ax^* + Lv^*, \quad 0 = f_{\mathrm{p}}(\bar{x}^*, w^*), \tag{10}$$

and interaction signals

$$w^* := \Gamma x^*, \quad v^* := g_{\mathrm{p}}(\bar{x}^*, w^*). \tag{11}$$

Due to the unavailability of the detailed representation of the environment $\overline{G}$, we consider its approximate modeling. The approximate linear static model of the environment is represented as

$$\overline{G}_{\mathrm{apx}} : v_{\mathrm{apx}} = v^* + \overline{\Theta}(w - w^*) \tag{12}$$

where $\overline{\Theta}$ is a learning parameter in the matrix form. The retrofit controller using the approximate linear model of the environment is described in the structure of

$$K(\overline{\Theta}) : \begin{cases} \dot{\hat{x}} = A\hat{x} + L\{v - \overline{\Theta}(w - \Gamma\hat{x})\} \\ u = \hat{K}(\overline{\Theta})(y - C\hat{x}). \end{cases} \tag{13}$$

The retrofit controller with the gain of $\hat{K}(\overline{\Theta})$ is designed to stabilize the feedback system G^+ in Fig. 1 consisting of the local linear subsystem G and the learning parameter $\overline{\Theta}$, which is given as

$$G^+ : \begin{cases} \dot{\hat{\xi}} = (A + L\overline{\Theta}\Gamma)\hat{\xi} + B\hat{u} \\ \hat{y} = C\hat{\xi}. \end{cases} \tag{14}$$

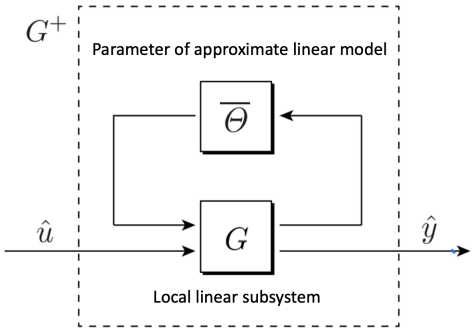

Fig. 1. Model for Retrofit Controller Design.

B. Environment Identification

In order to determine the learning parameter $\overline{\Theta}$ in (12), derivation of a linear static environment around an operating point of interest is proposed. We decompose $\overline{\Theta}$ as

$$\begin{aligned} \overline{\Theta} = & \underbrace{\left.\frac{\partial v}{\partial w}\right|_{(x^*, \bar{x}^*)}}_{\overline{\Theta}^{\mathrm{int}}} \\ & + \underbrace{\left.\frac{\partial v}{\partial |\boldsymbol{V}|}\frac{\partial |\boldsymbol{V}|}{\partial w}\right|_{(x^*, \bar{x}^*)} + \left.\frac{\partial v}{\partial \angle \boldsymbol{V}}\frac{\partial \angle \boldsymbol{V}}{\partial w}\right|_{(x^*, \bar{x}^*)}}_{\overline{\Theta}^{\mathrm{ext}}}, \end{aligned} \tag{15}$$

where the first part $\overline{\Theta}^{\mathrm{int}}$ corresponds to a local feedback effect, and the second part $\overline{\Theta}^{\mathrm{ext}}$ corresponds to a global feedback effect via the bus voltage phasor.

IV. Main Results: Data-Adaptive Retrofit Control Using Park Generator Model

A. Particular System Description for Retrofit Control

We describe the details of an extended data-adaptive retrofit control with the Park generator model. The internal states of the local linear subsystem G and interaction signals in (8) can be described as

$$x = \begin{bmatrix} \delta \\ \omega \\ E_{\mathrm{q}} \\ E_{\mathrm{d}} \\ \psi_{\mathrm{q}} \\ \psi_{\mathrm{d}} \\ V_{\mathrm{fd}} \\ x_{\mathrm{pss1}} \\ x_{\mathrm{pss2}} \\ x_{\mathrm{pss3}} \end{bmatrix}, \quad v := \begin{bmatrix} P_{\mathrm{m}}^* - P \\ E_{\mathrm{fd}} \\ E_{\mathrm{fq}} \\ \psi_{\mathrm{qs}} \\ \psi_{\mathrm{ds}} \\ |V| \end{bmatrix}, \quad w := \begin{bmatrix} \delta \\ \omega \\ E_{\mathrm{q}} \\ E_{\mathrm{d}} \\ \psi_{\mathrm{q}} \\ \psi_{\mathrm{d}} \end{bmatrix} \tag{16}$$

where P is defined as in (1a)-(1c), and $E_{\mathrm{fd}}, E_{\mathrm{fq}}, \psi_{\mathrm{qs}}, \psi_{\mathrm{ds}}$ are defined as

$$\begin{aligned} E_{\mathrm{fd}} &= E_{\mathrm{q}} + (X_{\mathrm{d}} - X'_{\mathrm{d}})\Big[I_{\mathrm{d}} - \tfrac{X'_{\mathrm{d}} - X''_{\mathrm{d}}}{(X'_{\mathrm{d}} - X_{\mathrm{ls}})^2}\{\psi_{\mathrm{d}} + \\ &\qquad (X'_{\mathrm{d}} - X_{\mathrm{ls}})I_{\mathrm{d}} - E_{\mathrm{q}}\}\Big] \\ E_{\mathrm{fq}} &= E_{\mathrm{d}} - (X_{\mathrm{q}} - X'_{\mathrm{q}})\Big[I_{\mathrm{q}} - \tfrac{X'_{\mathrm{q}} - X''_{\mathrm{q}}}{(X'_{\mathrm{q}} - X_{\mathrm{ls}})^2}\{\psi_{\mathrm{q}} + \\ &\qquad (X'_{\mathrm{q}} - X_{\mathrm{ls}})I_{\mathrm{q}} + E_{\mathrm{d}})\}\Big] \\ \psi_{\mathrm{qs}} &= -\psi_{\mathrm{q}} - E_{\mathrm{d}} - (X'_{\mathrm{q}} - X_{\mathrm{ls}})I_{\mathrm{q}} \\ \psi_{\mathrm{ds}} &= -\psi_{\mathrm{d}} + E_{\mathrm{q}} - (X'_{\mathrm{d}} - X_{\mathrm{ls}})I_{\mathrm{d}}. \end{aligned} \tag{17}$$

The system matrices A, B, Γ, and L are described in (18) while the input u corresponds to $V_{\mathrm{pss,re}}$ in (5) which is the control input produced by a local PSS designed by retrofit control approach.

$$A = \begin{bmatrix} 0 & \omega_0 & 0\,0\,0\,0 & 0 & 0 & 0 & 0 \\ 0 & -\frac{D}{M} & 0\,0\,0\,0 & 0 & 0 & 0 & 0 \\ 0 & 0 & 0\,0\,0\,0 & \frac{1}{T'_{\mathrm{do}}} & 0 & 0 & 0 \\ 0 & 0 & 0\,0\,0\,0 & 0 & 0 & 0 & 0 \\ 0 & 0 & 0\,0\,0\,0 & 0 & 0 & 0 & 0 \\ 0 & 0 & 0\,0\,0\,0 & 0 & 0 & 0 & 0 \\ 0 & \frac{D_{\mathrm{pss}}k_{ap}}{\tau} & 0\,0\,0\,0 & -\frac{1}{\tau} & \frac{C_{\mathrm{pss}}k_{\mathrm{ap}}}{\tau} & & \\ 0 & B_{\mathrm{pss}} & 0\,0\,0\,0 & 0 & A_{\mathrm{pss}} & & \\ 0 & & 0\,0\,0\,0 & 0 & & & \end{bmatrix},$$

$$B = \begin{bmatrix} 0 \\ 0 \\ 0 \\ 0 \\ 0 \\ 0 \\ -\frac{k_{\mathrm{ap}}}{\tau} \\ 0 \\ 0 \\ 0 \end{bmatrix}, \Gamma = \begin{bmatrix} 1&0&0&0&0&0&0&0&0&0 \\ 0&1&0&0&0&0&0&0&0&0 \\ 0&0&1&0&0&0&0&0&0&0 \\ 0&0&0&1&0&0&0&0&0&0 \\ 0&0&0&0&1&0&0&0&0&0 \\ 0&0&0&0&0&1&0&0&0&0 \end{bmatrix}, \tag{18}$$

$$L = \begin{bmatrix} 0 & 0 & 0 & 0 & 0 & 0 \\ \frac{1}{M} & 0 & 0 & 0 & 0 & 0 \\ 0 & -\frac{1}{T'_{\mathrm{do}}} & 0 & 0 & 0 & 0 \\ 0 & 0 & -\frac{1}{T'_{\mathrm{qo}}} & 0 & 0 & 0 \\ 0 & 0 & 0 & -\frac{1}{T''_{\mathrm{do}}} & 0 & 0 \\ 0 & 0 & 0 & 0 & -\frac{1}{T''_{\mathrm{qo}}} & 0 \\ 0 & 0 & 0 & 0 & 0 & -\frac{k_{\mathrm{ap}}}{\tau} \\ 0 & 0 & 0 & 0 & 0 & 0 \\ 0 & 0 & 0 & 0 & 0 & 0 \\ 0 & 0 & 0 & 0 & 0 & 0 \end{bmatrix},$$

B. Environment Identification

The proposal of the environment identification algorithms using the Park generator model described below is one of the main contributions of this paper. The local feedback effect matrix $\overline{\Theta}^{int}$ in (15) can be described as

$$\overline{\Theta}^{\mathrm{int}} := \left[\frac{\partial v}{\partial \delta} \quad \frac{\partial v}{\partial \omega} \quad \frac{\partial v}{\partial E_{\mathrm{q}}} \quad \frac{\partial v}{\partial E_{\mathrm{d}}} \quad \frac{\partial v}{\partial \psi_{\mathrm{q}}} \quad \frac{\partial v}{\partial \psi_{\mathrm{d}}} \right] \Big|_{(x^*, \bar{x}^*)}. \tag{19}$$

Although an explicit representation is omitted, a standard numerical tool can be used to find the Jacobian matrix. The global feedback effect matrix $\overline{\Theta}^{\mathrm{ext}}$ in (15) is described as

$$\overline{\Theta}^{\mathrm{ext}} = \left[\frac{\partial v}{\partial |\boldsymbol{V}|} \quad \frac{\partial v}{\partial \angle \boldsymbol{V}|} \right] \Big|_{(x^*, \bar{x}^*)} \hat{\theta} \tag{20}$$

where $\hat{\theta}$ is an estimated value of

$$\theta := \begin{bmatrix} \frac{\partial |\boldsymbol{V}|}{\partial \delta} & \frac{\partial |\boldsymbol{V}|}{\partial \omega} & \frac{\partial |\boldsymbol{V}|}{\partial E_{\mathrm{q}}} & \frac{\partial |\boldsymbol{V}|}{\partial E_{\mathrm{d}}} & \frac{\partial |\boldsymbol{V}|}{\partial \psi_{\mathrm{q}}} & \frac{\partial |\boldsymbol{V}|}{\partial \psi_{\mathrm{d}}} \\ \frac{\partial \angle \boldsymbol{V}}{\partial \delta} & \frac{\partial \angle \boldsymbol{V}}{\partial \omega} & \frac{\partial \angle \hat{\boldsymbol{V}}}{\partial E_{\mathrm{q}}} & \frac{\partial \angle \hat{\boldsymbol{V}}}{\partial E_{\mathrm{d}}} & \frac{\partial \angle \hat{\boldsymbol{V}}}{\partial \psi_{\mathrm{q}}} & \frac{\partial \angle \hat{\boldsymbol{V}}}{\partial \psi_{\mathrm{d}}} \end{bmatrix} \Big|_{(x^*, \bar{x}^*)} \tag{21}$$

From the initial tests, we have empirically found that the magnitude and the phase of the bus voltage phasor are significantly influenced by internal voltages and the rotor angle respectively. Therefore, we estimate the values of θ_1 to θ_5 in (22) while the rest of the values are supposed to be zero.

$$\begin{aligned} \theta_1 &:= \frac{\partial |\boldsymbol{V}|}{\partial E_{\mathrm{q}}}(x^*, \bar{x}^*), \quad \theta_2 := \frac{\partial \angle \boldsymbol{V}}{\partial \delta}(x^*, \bar{x}^*), \\ \theta_3 &:= \frac{\partial |\boldsymbol{V}|}{\partial E_{\mathrm{d}}}(x^*, \bar{x}^*), \quad \theta_4 := \frac{\partial |\boldsymbol{V}|}{\partial \psi_{\mathrm{q}}}(x^*, \bar{x}^*), \\ \theta_5 &:= \frac{\partial |\boldsymbol{V}|}{\partial \psi_{\mathrm{d}}}(x^*, \bar{x}^*), \end{aligned} \tag{22}$$

We present two distinct methods for numerical estimation of the values in (22), both following the same steps from 1 to 3, with variations in Step 4 for each method.

Step 1: The generator owner obtains measurements of the state variables of the standard PSS during an external disturbance to produce V_{pss} according to (4), which will be used as an excitation input in the later steps. For clarification, this external input will be denoted as $\hat{V}_{\mathrm{pss}}(t)$.

Step 2: The generator owner acquires a data set of the actual generator states by injecting an excitation input to the AVR connected to the generator of interest. Instead of an artificial random input, we use $\hat{V}_{\mathrm{pss}}(t)$ from Step 1 to simulate a realistic disturbance. The resultant time series data of $\delta(t), \omega(t), E_{\mathrm{q}}(t), E_{\mathrm{d}}(t), \psi_{\mathrm{q}}(t)$ and $\psi_{\mathrm{d}}(t)$ will be recorded and used as a reference for optimization.

Step 3: Using the same input $\hat{V}_{\mathrm{pss}}(t)$ as $\hat{u}$ in (14), the generator owner acquires estimated time series data of $\hat{\delta}(t), \hat{\omega}(t), \hat{E}_{\mathrm{q}}(t), \hat{E}_{\mathrm{d}}(t), \hat{\psi}_{\mathrm{q}}(t)$ and $\hat{\psi}_{\mathrm{d}}(t)$. Note that the learning parameter $\overline{\Theta}$ requires allocation of θ_1 to θ_5 values in (22), the process of which will be described in Step 4.

Step 4: We decide the values of θ_1 to θ_5 using time series data from Step 2 and Step 3.

(Algorithm A) This algorithm aims to follow the same optimization process as that in the one-axis generator model [10] by using only the principal states in the Park generator model. Therefore, the generator owner sets θ_3, θ_4 and θ_5 as zero. Then, the generator owner optimizes θ_1 with temporary value of θ_2 by minimizing the following objective function:

$$Q_{E\mathrm{q}}(\theta_1, \theta_2, 0, 0, 0) := \sqrt{\int_{t_1}^{t_2} |E_{\mathrm{q}}(t) - \hat{E}_{q\theta}(t)|^2 dt}. \tag{23}$$

Moreover, optimization of θ_2 follows the same process with temporary value of θ_1 by minimizing the following objective function:

$$Q_{\delta}(\theta_1, \theta_2, 0, 0, 0) := \sqrt{\int_{t_1}^{t_2} |\delta(t) - \hat{\delta}_{\theta}(t)|^2 dt}. \tag{24}$$

The generator owner repeats the optimization of θ_1 and θ_2 until the values from both processes converge. For reference, using the IEEE 68-bus system, the generator owners at Bus 2 and Bus 16 individually obtain the converged values of θ_1 and θ_2 given in Table I.

(Algorithm B) Data-adaptive PSS using Algorithm B involves optimization of five variables and two minimum

TABLE I
ESTIMATED VALUE FROM ALGORITHM A

Bus No.	θ_{1A}	θ_{2A}	θ_{3A}	θ_{4A}	θ_{5A}
2	0.3158	0.2632	0.000	0.000	0.000
16	0.9474	0.8421	0.000	0.000	0.000

TABLE II
ESTIMATED VALUE FROM ALGORITHM B

Bus No.	θ_{1A}	θ_{2A}	θ_{3A}	θ_{4A}	θ_{5A}
2	0.4771	0.4653	0.9043	0.3238	0.0896
16	0.0194	0.6692	0.1539	0.9893	0.4778

objective functions in the Park generator model. We define the two objective functions as

$$\begin{aligned} Q_{\mathrm{E_q}}(\theta_1,\theta_2,\theta_3,\theta_4,\theta_5) &:= \sqrt{\int_{t_1}^{t_2} |E_{\mathrm{q}}(t) - \hat{E}_{q\theta}(t)|^2 dt}, \\ Q_{\delta}(\theta_1,\theta_2,\theta_3,\theta_4,\theta_5) &:= \sqrt{\int_{t_1}^{t_2} |\delta(t) - \hat{\delta}_{\theta}(t)|^2 dt}. \end{aligned} \tag{25}$$

We employ a controlled and elitist Genetic Algorithm (GA) for multi-objective optimization [18] to obtain a pareto set. We propose the following prioritization rule to choose the best values from the pareto set. We propose to prioritize the error minimization of the generator's rotor angle during the light load condition. However, during the heavy load condition, E_q values are predominantly higher, causing high error sensitivity. Therefore, we propose to prioritize the error minimization of the internal voltage due to field winding during the heavy load condition.

For reference, using the default multi-objective Genetic Algorithm from MATLAB Global Optimization Toolbox with 100 generations and a population size of 100, the generator owners at Bus 2 and Bus 16 obtain the optimized values given in Table II.

V. NUMERICAL SIMULATION

In this section, we demonstrate the efficacy of the data-adaptive PSS through a detailed numerical simulation of the IEEE 68-bus test system, which consists of 16 Park generator models, resulting in a 160-dimensional DAE. The presentation of this large-scale and complex numerical demonstration is the second contribution of this paper. All the generators in the IEEE 68-bus system are equipped with the standard PSS in (4) and AVR in (5) without the data-adaptive PSS input, designed with the parameters given in Table III. All loads are represented as the constant impedance model given in (6).

A. Implementation of Single Refined PSS

Given the parameters of the IEEE 68-bus system model, the generator owners are positioned at Bus 2 and Bus 16 to assess the effectiveness of the data-adaptive PSS during light load and heavy load condition respectively. Supposing that the power system is operated at equilibrium, we model the local feedback effect in (19) for each Bus. Using the values

TABLE III
PARAMETERS OF STANDARD PSS AND AVR

Bus No.	k_{ap}	τ	K_{pss}	τ_{pss}	$\tau'_{\mathrm{L1}}, \tau'_{\mathrm{L2}}$	$\tau_{\mathrm{L1}}, \tau_{\mathrm{L2}}$
1	100	0.002	250	10	0.07	0.02
2-12	70	0.002	250	10	0.07	0.02
13-14	60	0.002	250	10	0.07	0.02
15	50	0.002	250	10	0.07	0.02
16	60	0.002	250	10	0.07	0.02

from Table I and Table II, we can model global feedback effect in (20) for each Bus. Then, with the availability of the learning parameter $\overline{\Theta}$, the feedback gain $\hat{K}(\overline{\Theta})$ in (13) is designed as an LQR. We perform the numerical simulation where only the generator of interest is attached with an AVR with refined PSS as described in (5).

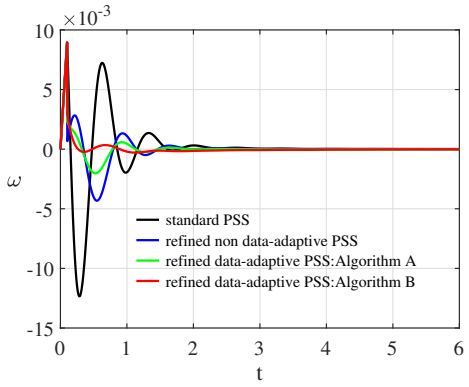

Fig. 2. Resultant angular frequency deviations at Bus 2 showing efficacy of refined PSS

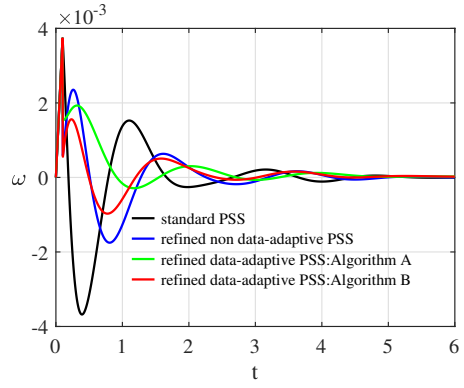

Fig. 3. Resultant angular frequency deviations at Bus 16 showing efficacy of refined PSS

Figs. 2 and 3 show the resultant time responses of the angular frequency deviations for a fault occurrence between 0 & 0.1 seconds at Bus 2 and Bus 16 respectively. The blue line response labeled with "refined non data-adaptive PSS" is obtained by setting the data-adaptive model $\overline{\Theta}^{\mathrm{ext}}$ to zero while the green and red responses labeled with "refined data-adaptive PSS" are obtained by optimizing $\overline{\Theta}^{\mathrm{ext}}$. The black line response is obtained by using a standard PSS only.

We confirm that during the light load condition, the refined data-adaptive PSS can be effectively designed using the

influence of the principal states not only in the one-axis generator model, but also in the Park generator model. On the other hand, during the heavy load condition where the effects of the rest of the states become significant, Algorithm A may lose its effectiveness.

B. Implementation of Multiple Refined PSSs

One significant advantage of data-adaptive retrofit control is the robust stability of the entire power system network, during parallel implementation of multiple PSSs. Therefore, we conduct numerical simulation where all 16 generators in the IEEE 68-bus model are equipped with respective refined PSSs. Given the parameters of the IEEE 68-bus model, we consider Bus 1 to Bus 11 as light load conditions while Bus 12 to Bus 16 are considered as heavy load conditions. We use the evaluation method based on [14] by denoting the angular frequency deviations of all generators as $\omega := (\omega_1, \ldots, \omega_{16})$ and draw the box plots of $\{\|\omega^{(i)}\|_2\}_{i=1}^{16}$ in Fig. 4 where $\omega^{(i)}$ represents the resultant deviations during the fault occurrence between 0 & 0.1 seconds at Bus i.

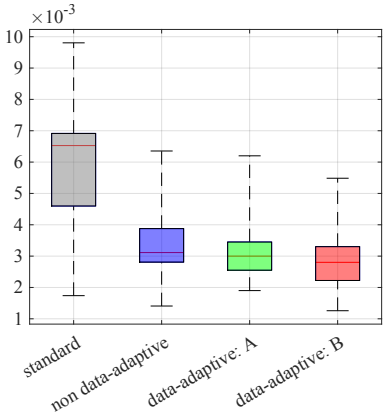

Fig. 4. Box plots of the magnitude of angular frequency deviations for each method when all the generators are equipped with refined PSS

The top and bottom black lines of Fig. 4 represent the maximum and the minimum while the red line represents the median of each box plot. Fig. 4 shows that the refined data-adaptive PSS using Algorithm B provides the overall performance enhancement during parallel implementation of multiple PSSs that are independently designed based on local subsystem models and measurements. It also shows that refined data-adaptive PSS using algorithm A, without considering the effects of all variables of the Park generator model in environment identification, can lead to deficiency in the overall performance.

VI. Concluding Remarks

We have extended the design of data-adaptive PSS from using the one-axis generator model to using the Park generator model in the framework of retrofit control. To address the higher order dynamics and increased states of the Park generator model, we proposed two methods for environment identification. One method utilizes only the effects of the principal states, while the other considers that of all the available states in the Park generator model. We remark that the data-adaptive PSS using the algorithm with the consideration of the effects of all the states of the Park generator model provides overall performance enhancement. Additionally, it is noteworthy this algorithm delivers the best performance, especially during heavy load conditions. Finally, we validated the efficacy of the data-adaptive PSS using the Park generator model during parallel implementation through numerical simulations on the IEEE 68-bus model.

Acknowledgement

This research was supported by JST-Mirai Program 18077648.

References

[1] *IEEE Recommended Practice for Excitation System Models for Power System Stability Studies*, 2016.

[2] P. Kundur, *Power System Stability and Control*. McGraw-Hill Education, 1994.

[3] F. Tito, G. Taranto, and P. Pellanda, "A robust power system control design combining system identification and genetic algorithms," in *Proceedings of the 1998 American Control Conference. ACC (IEEE Cat. No.98CH36207)*, vol. 6, 1998, pp. 3403–3407 vol.6.

[4] M. A. Abido and Y. L. Abdel-Magid, "Robust design of multimachine power system stabilisers using tabu search algorithm," *IEE Proceedings: Generation, Transmission and Distribution*, vol. 147, pp. 387–394, 2000.

[5] M. A. Abido, "Optimal design of power-system stabilizers using particle swarm optimization," *IEEE Transactions on Energy Conversion*, vol. 17, pp. 406–413, 9 2002.

[6] F. Jamsheed and S. J. Iqbal, "Design of an adaptive power system stabilizer using robust system-response prediction," in *2020 IEEE International Conference on Power Electronics, Smart Grid and Renewable Energy (PESGRE2020)*, 2020, pp. 1–6.

[7] A. A. Canabal, A. G. Loukianov, J. M. C. Castañeda, and V. A. Utkin, "Adaptive power system stabilizer with sliding mode for electric power systems," *International Journal of Electrical Power & Energy Systems*, vol. 145, p. 108700, 2023.

[8] Y.-M. Park, M.-S. Choi, and K. Lee, "A neural network-based power system stabilizer using power flow characteristics," *IEEE Transactions on Energy Conversion*, vol. 11, no. 2, pp. 435–441, 1996.

[9] P. Shamsollahi and O. Malik, "Application of neural adaptive power system stabilizer in a multi-machine power system," *IEEE Transactions on Energy Conversion*, vol. 14, no. 3, pp. 731–736, 1999.

[10] T. Ishizaki, M. Ito, T. Kawaguchi, and A. Chakrabortty, "Data-adaptive retrofit control for power system stabilizer design," in *2022 IEEE 61st Conference on Decision and Control (CDC)*, 2022, pp. 2210–2215.

[11] T. Ishizaki, T. Sadamoto, J. ichi Imura, H. Sandberg, and K. H. Johansson, "Retrofit control: Localization of controller design and implementation," *Automatica*, vol. 95, pp. 336–346, 2018.

[12] T. Sadamoto, A. Chakrabortty, T. Ishizaki, and J.-i. Imura, "Retrofit control of wind-integrated power systems," *IEEE Transactions on Power Systems*, vol. 33, no. 3, pp. 2804–2815, 2018.

[13] T. Ishizaki, T. Kawaguchi, H. Sasahara, and J. ichi Imura, "Retrofit control with approximate environment modeling," *Automatica*, vol. 107, pp. 442–453, 2019.

[14] T. Ishizaki, H. Sasahara, M. Inoue, T. Kawaguchi, and J. I. Imura, "Modularity in design of dynamical network systems: Retrofit control approach," *IEEE Transactions on Automatic Control*, vol. 66, pp. 5205–5220, 2021.

[15] P. W. Sauer, M. A. Pai, and J. H. Chow, *Power system dynamics and stability: with synchrophasor measurement and power system toolbox*. John Wiley & Sons, 2017.

[16] B. Pal and B. Chaudhuri, *Robust Control in Power Systems*. Springer-Verlag, 2006.

[17] T. Sadamoto, A. Chakrabortty, T. Ishizaki, and J. I. Imura, "Dynamic modeling, stability, and control of power systems with distributed energy resources: Handling faults using two control methods in tandem," *IEEE Control Systems*, vol. 39, pp. 34–65, 2019.

[18] M. Inc., *MATLAB Global Optimization Toolbox User's Guide*. Natick, Massachusetts, USA: version 9.14.0.2206163 (R2023a), 2023.